TAO, Vol. 17, No. 1, 179-202, March 2006

# A Review of the Source Parameters of the 1999 $M_s$7.6 Chi-Chi, Taiwan, Earthquake

Jeen-Hwa Wang[1,*]

(Manuscript received 3 January 2005, in final form 5 December 2005)


## ABSTRACT

**An $M_s$7.6 Chi-Chi earthquake, which ruptured the Chelungpu fault, struck central Taiwan on 20 September 1999 at 17:47 p.m. GMT. Observed data and inversion results lead to the estimated values of source parameters of the earthquake based on distinct methods for measurement or inversion. In this study, the values of several source parameters, including the surface ruptures, displacements on the fault plane, peak ground velocity (PGV), peak ground acceleration (PGA), predominant frequency ($f_o$), corner frequency ($f_c$), spectral level ($\Omega_o$), seismic moment ($M_o$), static stress drop ($\Delta\sigma_s$), dynamic stress drop ($\Delta\sigma_d$), rupture velocity ($V_R$), strained energy ($\Delta E$), seismic radiation energy ($E_s$), etc are reviewed. In addition, the observed source scaling law is also taken into account. Results show remarkable differences in source properties between the northern and southern segments of the Chelungpu fault.**


**(Key words: Chi-Chi earthquake, Source parameter)**

## 1. INTRODUCTION

Earthquake rupture processes are examples of the physics of complexity. Stress exerted by regional tectonics increases with time. When such a stress reaches the breaking strength, i.e., the static frictional stress of the fault zone, the frictional stress decreases with either velocity or displacement (cf. Wang 1996, 2002), and then the fault breaks, thus generating an earthquake. The frictional force in the fault plane and the coupling between the plates and the fault zone can resist the motions of the fault plane, and the stress in the fault zone then drops to

[1] Institute of Earth Sciences, Academia Sinica, Taipei, Taiwan, ROC

[*] *Corresponding author address:* Dr. Jeen-Hwa Wang, Institute of Earth Sciences, Academia Sinica, Taipei, Taiwan, ROC; E-mail: jhwang@earth.sinica.edu.tw

a final level, $\sigma_f$. Figure 1 displays the variation of stresses in the fault zone. After an earthquake rupture, the stress in the fault zone decreases from the initial level, $\sigma_o$, to the lowest dynamical friction level, $\sigma_d$, which is equal to or smaller than the final level, $\sigma_f$ (Kanamori and Heaton 2000). The actual friction law described by the dashed line, is approximated by a piece-wise linear function. In addition to these three parameters, seismologists also define other parameters to describe earthquakes. Source parameters include the surface ruptures, displacement in the fault plane, peak ground velocity, PGV, peak ground acceleration, PGA, predominant frequency ($f_o$), seismic moment ($M_o$), corner frequency ($f_c$), spectral level ($\Omega_o$), static stress drop ($\Delta\sigma_s$), dynamic stress drop ($\Delta\sigma_d$), average stress, $[\sigma_{av} = (\sigma_o + \sigma_f)/2]$, apparent stress ($\sigma_a$), strain energy ($\Delta E$), seismic radiation energy ($E_s$), fracture energy ($E_g$), frictional energy ($E_f$), etc. Based on these source parameters, seismologists develop source models, for example, the so-called $\omega$-squared or $\omega$-cubic source scaling law (Aki 1967; Brune 1970).

In the past, only limited information concerning the source parameters of a few earthquakes in Taiwan was given (Wang 1998). However, a complete data set of all source parameters is needed for either comprehensively understanding the source processes or mitigating

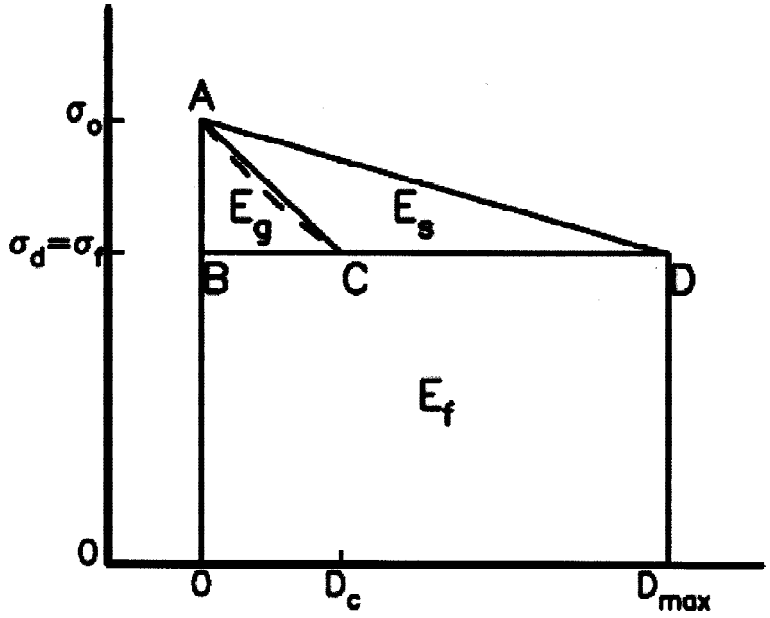


*Fig. 1.* The stress-slip function: dashed line AC (approximated by line AC) plus line CD represent slip-weakening friction, $D_c$ = the characteristic slip displacement, $D_{max}$ = the maximum slip, $\sigma_o$ = initial stress (or static frictional stress), $\sigma_d$ = dynamic frictional stress, and $\sigma_f$ = final stress. The strain energy, $\Delta E$, per unit area is the area of a trapezoid below line AD, $E_s$ = the seismic radiation energy, $E_g$ = fracture energy, and $E_f$ = frictional energy.

seismic hazards in the region. The $M_s$7.6 Chi-Chi earthquake struck central Taiwan on 20 September 1999 at 17:47 p.m. GMT (Ma et al. 1999; Shin 2000). The earthquake resulted from an over 80-kilometer-long, east-dipping thrust fault (Chelungpu fault), with a maximum vertical ground displacement of over 6 meters and with a maximum horizontal ground displacement of over 9 meters. The epicenter and the Chelungpu fault are shown in Fig. 2. High-quality accelerograms (Liu et al. 1999) generated by the earthquake were recorded at several seismic stations. Nine of the stations are very close to the fault trace (see Fig. 2). Since the occurrence of the Chi-Chi earthquake, numerous seismological, geophysical, geodetic, and geological observations have been made. Based on the data, the slip distribution of the earthquake was inferred by several groups of researchers through inversion techniques. All the results show a heterogeneous slip distribution on the fault plane and remarkable differences in source properties between the northern and southern segments of the Chelungpu fault. The two segments are almost separated at the middle of the fault. It is noted that the source parameters of several larger-sized aftershocks were also studied by a few researchers (Chan and Ma 2004; Chi and Dreger 2002, 2004; Huang et al. 2002).

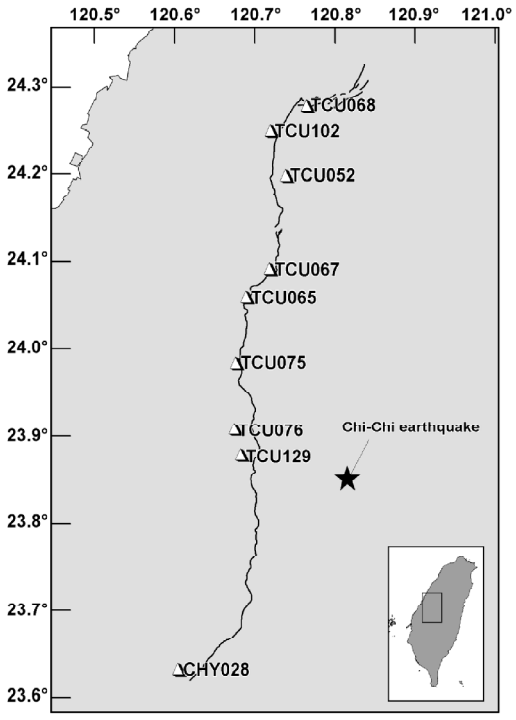


*Fig. 2*. The epicenter of the 21 September 1999 Chi-Chi earthquake is denoted by a solid star. The localities of nine near-fault seismic stations are displayed by solid triangles. The solid lines display the surface trace of the Chelungpu fault.

In this study, the values of several source parameters of the Chi-Chi mainshock, including the surface ruptures, displacements in the fault plane, peak ground velocity, peak ground acceleration, predominant frequency, seismic moment, corner frequency, spectral level, static stress drop, dynamic stress drop, average stress, apparent stress, strained energy, seismic radiation energy etc are reviewed. In addition, the measured $\omega$-squared source scaling law from near-fault seismograms will also be considered.

From measured and evaluated values of accelerations, velocities, and displacements, Wang (2003) stressed the difference in several source parameters between the northern and southern segments (Fig. 2), which are separated at a locality near TCU065. The capital letters 'N' and 'S' are, respectively, used to represent the northern and southern segments. Hwang and Wang (2002) found a difference in source scaling laws between the two segments. From trenching data, Wang (2005a) inferred different return periods for earthquakes between the two segments. Hence, in this review the differences in source parameters between the two segments will also be addressed.

## 2. DEFINITIONS AND MEASUREMENTS OF SOURCE PARAMETERS

The definitions and methods to measure or estimate the source scaling law and related parameters, including D, $D_{max}$, $f_o$, $f_c$, $\Omega_o$, $M_o$, $\Delta\sigma_s$, $\Delta\sigma_d$, $V_R$, $\Delta E$, $E_s$ etc, are described below:

(1) Average Displacement (D) and Maximum Displacement ($D_{max}$)

If an earthquake fault breaks the ground surface, geologists can directly measure surface ruptures. Otherwise, the displacements in the fault plane must be inferred from seismograms and/or crustal deformations using inversion techniques. D and $D_{max}$ denote, respectively, the average value and the maximum one over the fault plane from measured surface ruptures and inverted slip distribution.

(2) Predominant Frequency ($f_o$)

The rupture processes of an earthquake are like the vibration of any object, with a natural frequency, $f_o$. From a one-body dynamic system, which consists of a body with a mass m and linked by a spring with a constant K, driven an external force F, Wang (2003) obtained $f_o = (K/m)^{1/2}$ and assumed that the natural frequency of an earthquake or an asperity of a subevent is almost the predominant frequency, which is associated with the peak spectral amplitude, of the near-fault seismograms and can be estimated from the Fourier transformation of seismograms.

(3) Source Scaling Law, Corner Frequency ($f_c$), and Spectral Level ($\Omega_o$)

The body-wave earthquake source spectrum of a displacement is controlled by the low-frequency spectral level, $\Omega_o$, which is associated with the seismic moment $M_o$, and corner frequency, $f_c$, which is the frequency, at which the spectral amplitudes obviously change. When $f < f_c$, the spectral amplitudes are almost constant; while when $f > f_c$, the spectral amplitude usually decays in a power-law function of $f^{\alpha}$, where "$\alpha$" is the exponent. Commonly accepted power-law functions have either $f^{-2}$ or $f^{-3}$ decaying at high frequencies. The

two functions are generally, respectively, referred to as the $\omega$-square and $\omega$-cubic models, where $\omega = 2\pi f$, (Aki 1967; Brune 1970). From observations, some authors prefer the $\omega$-square model (cf. Aki 1967; Anderson 1984), while others support the $\omega$-cubic one (cf. Frasier and North 1978; Patane et al. 1997). Of course, some others (cf. Fletcher 1980; Boatwright 1978; Dysart et al. 1988) have claimed that neither is appropriate to describe the observations. The two parameters $f_c$ and $\Omega_o$ are, in general, visually estimated directly from the displacement spectra. However, this can lead to a high level of uncertainty. Some seismologists (e.g., Andrews 1986) use nonlinear method to eliminate the uncertainty.

Let d(t), v(t), and a(t) be the time functions of the displacement, velocity and acceleration, respectively. Their Fourier transforms are, respectively, D(f), V(f), and A(f). According to the $\omega$-squared source model, the approximations of the three frequency-dependent functions are, respectively:

$$D(f) = \Omega_o / [1 + (f/f_c)^2] \quad , \tag{1}$$

$$V(f) = 2\pi f \Omega_o / [1 + (f/f_c)^2] \quad , \tag{2}$$

and

$$A(f) = (2\pi f)^2 \Omega_o / [1 + (f/f_c)^2] \quad . \tag{3}$$

The three expressions lead to the following approximations: (1) $D(f) \sim f^0$, $V(f) \sim f^1$, and $A(f) \sim f^2$ when $f << f_c$; and (2) $D(f) \sim f^{-2}$, $V(f) \sim f^{-1}$, and $A(f) \sim f^0$ when $f >> f_c$. Hence, Eqs. (1) - (3) can be individually approximated by a set of two piece-wise linear functions as displayed in Fig. 3.

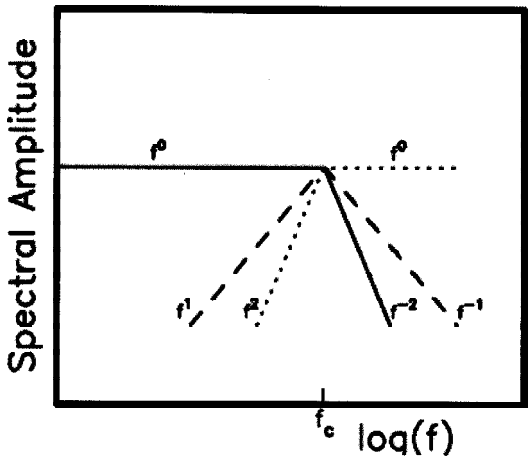


*Fig. 3*. The simplified theoretical spectra for the displacement (in the solid lines), velocity (in the dashed lines), and acceleration (in the dotted lines).

(4) Seismic Moment ($M_o$)

The seismic moment can be calculated from the following formula (Aki and Richard 1980):

$$M_o = 4\pi[\rho(\xi)\rho(x)c(x)]^{1/2}c(\xi)^{5/2}r\Omega_o/R_{\theta\phi} \quad . \tag{4}$$

In Eq. (4), $\rho$, and c are, respectively, the density and P- or S-wave velocity, while $\xi$ and x express, respectively, the source region and the area around the seismic station. Other quantities are: r = the hypocentral distance or the distance between an asperity and a station site and $R_{\theta\phi}$ = the radiation pattern, where $\theta$ is the take-off angle of the rays emitted from the fault plane and $\phi$ is the strike angle. The value of $R_{\theta\phi}$ must be estimated from a focal-plane solution. When the focal-plane solution of an earthquake is unknown, an average of $R_{\theta\phi}$ is taken: 0.52 for the P waves and 0.63 for the S waves (Boore and Boatwright 1984). For a homogeneous and isotropic space, Aki (1966) obtained $M_0 = \mu DA$, where $\mu$ and A are the rigidity and the fault area, respectively. The value of $\mu$ is usually $3\times10^{11}$ dyne $cm^{-2}$ for the crustal materials.

(5) Static Stress Drop ($\Delta\sigma_s$) and Dynamic Stress Drop ($\Delta\sigma_d$)

From Fig. 1, two parameters, i.e., the static stress drop $\Delta\sigma_s = \sigma_o - \sigma_f$ and the dynamic stress drop $\Delta\sigma_d = \sigma_o - \sigma_d$, are defined to show the change of stresses during faulting of an earthquake. Boatwright (1980, 1984) proposed a model to describe the dynamic stress drop in the beginning stage of faulting. The expression is:

$$\Delta\sigma_d = M_o(1-\xi^2)(V_o/t)/4\pi\Omega_o V_R{}^3 \quad . \tag{5}$$

In Eq. (5), $V_o/t$ expresses the slope of the initial pulse of a velocity seismogram and $\xi = (V_R/c)\sin\theta$, where c is the body-wave velocity and $V_R$ is the rupture velocity and about equal to $0.8\beta$, where $\beta$ is the S-wave velocity.

(6) Rupture Velocity ($V_R$)

After an earthquake initiates, the ruptures spread from the hypocenter. The rupture velocity can vary from one location to another, because of an inhomogeneous fault plane. In order to simplify the problem, a constant rupture velocity is commonly given to the entire fault of a small earthquake or to a portion of a large event. Hence, for a large event like the Chi-Chi earthquake $V_R$ is not constant.

(7) Energies

The strain energy ($\Delta E$) due to tectonic loading releases after faulting. The faulting process is usually complex and only a simplified one as shown in Fig. 1 is taken into account. $\Delta E$ is expressed by the area of the trapezoid underneath the linear decreasing function of stress versus slip, i.e., $\Delta E = (\sigma_o + \sigma_f)DA/2$. A complete definition of $\Delta E$ can be described as below (Knopoff 1958):

$$\Delta E = \int u_i(\sigma_{oij} + \sigma_{fij})\nu_j dA \quad , \tag{6}$$

where $u_i$ is the slip along the i-th axis, $\nu_j$ is the unit vector normal to the fault plane and along the j-th axis, and $\sigma_{oij}$ and $\sigma_{fij}$ are, respectively, the initial and final stress tensors. For details of the methodology to measure the $\Delta E$ see Wang (2004), only a brief description is give below. Excluding the rotation components, the approximation of Eq. (6) is $\Delta E = \mu[(u_L/l_L)u_L + (u_W/l_W)u_W]A$, where $u_L$ and $u_W$ denote the average displacements along the fault-striking (L) direction and the fault-dipping (W) one, respectively, and $l_L$ and $l_W$ are the length and width of an area in consideration along the two directions. In the approximation, Wang (2004) took $d^2\sigma_L/dx^2 \approx 0$ and $d^2\sigma_W/dx^2 \approx 0$ under the assumption that the stress field is uniform within the space domain in use.

$\Delta E$ will be transferred into, at least, three parts (Fig. 1), that is $\Delta E = E_s + E_g + E_f$, where $E_s$ = seismic radiation energy, $E_g$ = fracture energy, and $E_f$ = frictional energy. It is not easy to preciously evaluate the value of $\Delta E$, unless there is a complete data set of crustal deformations. The $E_s$ is the kinetic energy emitted from the earthquake source through seismic waves during faulting, and can be measured based on Eq. (10) as mentioned below. In general, $E_s$ is about $(10-20)\%\,\Delta E$ (cf. Wang 2004). The $E_g$ is used to extend the two surfaces of the fault plane and can also be estimated from seismic data from the following expression:

$$E_g = [(1 - V_R/\beta)/(1 + V_R/\beta)]^{1/2}\Delta\sigma_d DA/2 \quad , \tag{7}$$

(Kanamori and Heaton 2000). Its value is small and usually ignored, because $V_R/\beta$ is usually in the range 0.75 - 0.85. The $E_f$ is produced by frictional sliding and can generate heat in the fault zone during faulting of an earthquake. When the values of $\Delta E$, $E_s$ and $E_g$ are given, $E_f$ can be calculated. Frictional energy would raise the temperature of the fault zone. From $E_f$, the heat could be ideally calculated when the thermal properties of the fault zone are known. Due to a lack of a complete data set, there is still high uncertainty in measuring energies, especially for $E_g$ and $E_f$. Hence, in this work only the results of $\Delta E$ and $E_s$ are considered.

There are numerous ways to estimate the source parameters. According to the $\omega$-squared source model, Andrews (1986) proposed an objective way. First, he defined two quantities:

$$I_D = \int d^2(t)dt = 2\int D^2(f)df \quad , \tag{8}$$

and

$$I_V = \int v^2(t)dt = 2\int V^2(f)df \quad . \tag{9}$$

In Eqs. (8) and (9), the Parseval theorem is applied to link the integrals in the time and frequency domains. In the two expressions, integration is, in principle, performed from $-\infty$ and $+\infty$ in the time domain and from 0 to $\infty$ in the frequency domain. In fact, integration can be made only in a finite frequency band, and, thus, the effect due to finite frequency bandwidth limitation exists. Wang (2004) and Wang and Huang (2005) theoretically studied such an

effect on the estimate of $E_s$.

Based on Andrews' method, several source parameters are measured through the following expressions:

(1) For $E_s$:

$$E_s = S_a \rho \beta I_V / (FR_{\theta\phi})^2 \quad . \tag{10}$$

(4) For $M_0$:

$$M_0 = 4\pi r \rho \beta^3 2 I_V^{-1/4} I_D^{3/4} \quad . \tag{11}$$

(5) For $\Delta\sigma_d$:

$$\Delta\sigma_d = 2\pi r \rho I_V^{5/4} I_D^{-3/4} / 2.34 \quad . \tag{12}$$

In Eqs. (10) - (12), $S_a = 4\pi r^2$ is the area of the sphere of the wave front at a hypocentral distance of r and F is the ground surface amplification factor. Several factors, including the seismic radiation pattern and surface amplification, and seismic-wave attenuation, will influence the estimates of the source parameters. Hwang et al. (2001a) took the ground surface amplification factor to be $F \fallingdotseq 2$ for the S waves. Because of the absence of detailed individual focal mechanisms associated with the two segments of the fault and a uneven distribution of stations, an average radiation pattern with a value of 0.63 for the S-waves was adopted by Hwang et al. (2001a) to adjust the amount of seismic radiation caused by a non-uniform seismic-wave radiation pattern (cf. Boore and Boatwright 1984). Due to a lack of frequency-dependent $Q_s$ value in the study area, only the average $Q_s$ value of 250 (Rau et al. 1996) was used by Hwang et al. (2001a) to correct the attenuation effect.

## 3. RESULTS

Presently, numerous earth scientists have studied the source parameters of the Chi-Chi earthquake through direct measurements or inversion techniques. In this work, the estimated values of D, $D_{max}$, $f_o$, $f_c$, $\Omega_o$, $M_o$, $\Delta\sigma_s$, $\Delta\sigma_d$, $V_R$, $\Delta E$, $E_s$ etc. will be reviewed. In addition, the source scaling law of the earthquake is also presented. Results are given below:

(1) Average Displacement (D) and Maximum Displacement ($D_{max}$)

Field surveys reported a larger surface ruptures in the northern segment than in the southern one and the hanging wall moved more than the footwall (CGS 1999; Lin et al. 2001; Chen et al. 2004). The measured surface displacements are 1.0 - 11.1 m horizontally and 2 - 7.5 m vertically, with the largest being 11.1 m horizontally and 7.5 m vertically in the north. From twice-integration of the near-fault accelerograms, Chung and Shin (1999) reported that $D_{max}$

is 8 m horizontally and 3.7 m vertically in the hanging wall and 1.3 m horizontally and 1 m vertically in the footwall. The displacements in the fault plane were also inferred through inversion techniques. Results showed a transition from predominantly thrust faulting in the south to largely left-lateral motion in the north. From teleseismic data, Kikuchi et al. (2000) obtained D = 3.1 m; and Xu et al. (2002) got $D_{max}$ = 6.5 m. From both local and teleseismic data, Ma et al. (2001) obtained $D_{max}$ = 12 m. From GPS data, Yoshioka (2001) obtained D = 5.1 m and $D_{max}$ = 13.8 m. From local seismic and GPS data, Wu et al. (2001) obtained $D_{max}$ = 20 m; and Zeng and Chen (2001) got D = 3.8 m and $D_{max}$ = 20 m. From local and teleseismic data plus GPS data, Ma et al. (2001) gave $D_{max}$ = 20 m, which is about 1.7 times larger than that inferred only from local and teleseismic data as mentioned above. Obviously, the GPS data affect the inference of source displacements. In addition, Lee and Ma (2002) reported an increase in $D_{max}$ from 6 m in the south to 10 m in the north using teleseismic data. Based on the source slip model inferred by Domingaez et al. (2003) from GPS and InSAR data, Wang (2005b) obtained the values of D on the northern and southern fault planes, i.e., $D_N$ = 7.15 m and $D_S$ = 4.88 m, and, thus, D = ($D_N$ + $D_S$)/2 = 6.02 m for the whole fault.

(2) Near-fault Accelerations and Velocities

From local accelerograms, Wen et al. (2001) reported that the largest PGA is greater than 1 g. Tsai and Huang (1999) and Brodsky and Kanamori (2001) stated smaller PGA and larger PGV at northern stations than at southern ones. In order to directly correlate the PGA and PGV with the orientation of the fault plane, Wang et al. (2002) rotated the acceleration waveforms at nine near-fault seismic stations from the original geographic system to one defined on the fault plane: the R-component along the fault-dipping direction and pointing to the west; the T-component along the fault-striking one, and the N-component being normal to the fault plane. Direct integration of the acceleration records leads to velocity waveforms. Wang et al. (2002) plotted the variations in the PGA and PGV of the rotated waveforms from south to north (Fig. 4). The symbols are: open circles for the R-component, crosses for the T-component, and open squares for the N-component. In addition, the data points for the footwall stations are connected by a solid line, and those for the hanging-wall stations are linked by a dashed line.

On the foot-wall side, the average PGA is about 250 cm $sec^{-2}$ at northern stations and about 600 cm $sec^{-2}$ at the southern ones; while the average PGV is about 65 cm $sec^{-1}$ at northern stations and about 60 cm $sec^{-1}$ at the southern ones at the foot wall. Unlike Wen et al. (2001), the largest PGA in the rotated waveforms is 275 cm $sec^{-1}$, which is less than 1 g, at the hanging wall. Fig. 4 shows that the PGA values are, on the average, smaller at the hanging wall than at the footwall, but opposite for the PGV values. At the footwall, TCU129, which is nearest the epicenter, recorded the largest PGA value along the R-component, and TCU065 gave large PGA values along the three components. Considering the seven footwall stations, the PGA value follows a similar variation, in which the PGA value decreases from the southernmost station to TCU075, with sudden increases at TCU065, and finally decreases again. On the other hand, the PGV values of the N- and R-components follow a similar variation, in which the PGV value increases from the southernmost station to TCU065 and then decreases. However, the PGV values of the T-component follow a slightly different variation, in which the PGV value somewhat increases from south to north. At the two hanging-wall stations, the

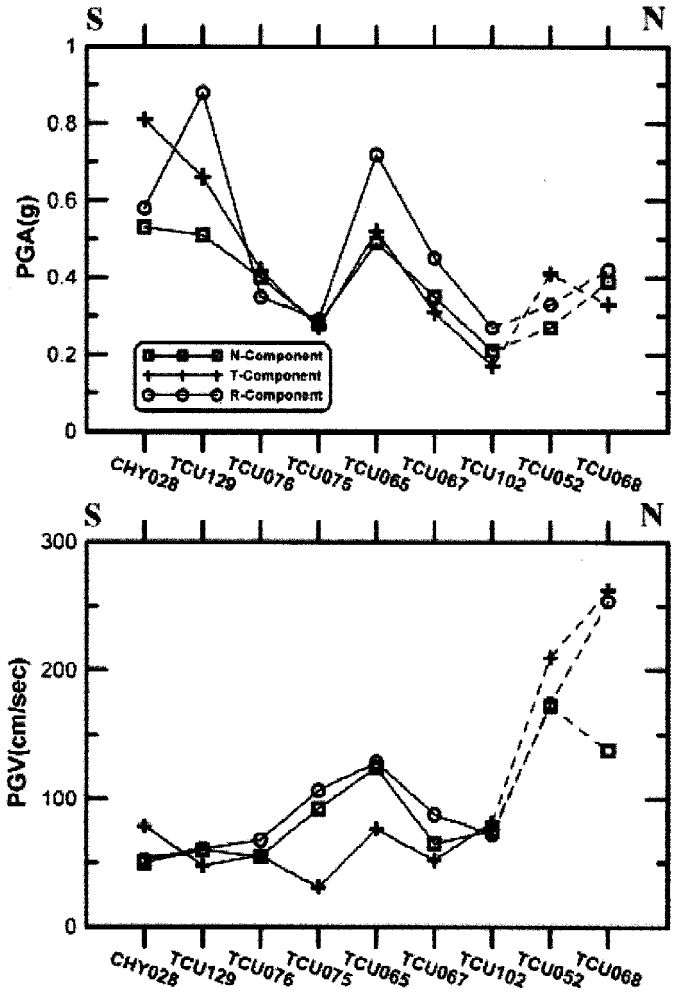


*Fig. 4.* (a) The variation in near-fault PGA from south to north and (b) The variation in near-fault PGV from south to north (Symbols: Open square for the N-component, cross for the T-component, and open circle for the R-component).

PGA values of the N- and R-components and the PGV values of the T- and R-components increase from south to north. Hence, for the footwall stations there are only minor differences in the PGV values between the northern and southern stations, and the PGV at the hanging wall are generally larger than those at the footwall. The difference in the PGA values between the hanging wall and the footwall is small, even though the PGA increases from north to south for both walls. At the northern stations, the PGA is slightly higher and the PGV is much larger at the hanging wall than at the footwall.

(3) Spectra and Predominant Frequency ($f_o$) of Near-fault Accelerograms

At nine near-fault seismic stations, Wang et al. (2002) Fourier transformed the rotated accelerograms to obtain acceleration spectra. It is obvious that the acceleration spectra vary from north to south. At the two stations nearest the epicenter, i.e., TCU129 and TCU076, and the southernmost station, i.e., CHY028, the higher- frequency spectral amplitudes are in general larger than the lower-frequency ones. The spectral amplitudes somewhat decrease from south to north when $f > 2$ Hz, and increase from south to north when $f < 1$ Hz. The spectral amplitudes have local peaks at $f \fallingdotseq 0.2$ Hz and at $f \fallingdotseq 1$ Hz, and the peak values somewhat increase from TCU129 to TCU065 and then decrease from TCU065 northward. At Station TCU065, large spectral amplitudes exist at the two frequencies. The spectral amplitudes in a large frequency band are greater at this station than at others. At the northernmost footwall station, i.e., TCU102, there is a strong signal with $f \fallingdotseq 0.4$ Hz in the T-component. When $f < 0.2$ Hz, there are large spectral amplitudes, especially for the T-component, at two hanging wall stations, i.e., TCU068 and TCU052, but weak at others. The acceleration spectra show that the value of $f_0$ is 1 Hz in the south and 0.2 Hz in the north.

(4) Source Scaling Law, Corner Frequency ($f_c$), and Spectral Level ($\Omega_o$)

Huang and Wang (2002) plotted the displacement spectra of the nine near-fault seismograms. The displacement spectra at four sites are shown in Fig. 5. Essentially, the $\omega$-squared source scaling law can describe the displacement spectra, except for the high-frequency range. In general, $f_c$ decreases and $\Omega_o$ increase from south to north. The average values of $f_c$ and $\Omega_o$ are, respectively, about 0.17 Hz and 97 cm-sec in the south and 0.12 Hz and 550 cm-sec in the north in the footwall and 0.064 Hz and 2350 cm-sec in the northern hanging wall. Nevertheless, as taking a closer look, the deviations of spectral amplitudes from the $\omega$-squared source scaling law are higher for the northern stations than for the southern ones. In the frequency range 0.2 - 3 Hz, Hwang and Wang (2002) stressed that the exponent $\beta$ of the power-law scaling relation of $P(\omega) \sim \omega^{-\beta}$ to describe the variation of spectral amplitudes, $P(\omega)$, in terms of angular frequency, $\omega$, varies station to station. The estimated values of $\beta$ for the nine near-fault stations vary from 1.63 to 3.04 from south to north: 2.78 ± 0.03 at TCU068, 2.91 ± 0.03 at TCU102, 3.04 ± 0.03 at TCU052, 2.23 ± 0.02 at TCU067, 2.63 ± 0.02 at TCU065, 2.26 ± 0.03 at TCU075, 2.08 ± 0.02 at TCU076, 1.87 ± 0.02 at TCU129 and 1.63 ± 0.02 at CHY028. The standard deviation at each station is smaller than 0.03. On the average, the scaling exponent is about 3 in the north and 2 in the south.

(5) Seismic Moment ($M_o$)

The values of $M_o$ estimated from teleseismic data are: (a) $2.4\times10^{20}$ Nm from the catalogue of USGS; (b) $4.1\times10^{20}$ Nm from the catalogue of Harvard University; (c) $0.5\times10^{20}$ Nm by Lee and Ma (2000); (d) $5\times10^{20}$ Nm by Yoshioka (2001); and (e) $2.8\times10^{20}$ Nm by Kikuchi et al. (2000). Obviously, the values are in the range of $(0.5 - 5)\times10^{20}$ Nm. There is a one-order-of-magnitude difference among the estimated values. From near-fault seismic data, the values of $M_o$ at four stations were estimated by Hwang et al. (2001a): $3.5\times10^{19}$ Nm at TCU102, $1.5\times10^{20}$ Nm at TCU052, $5.8\times10^{18}$ Nm at TCU076, and $5.3\times10^{18}$ Nm at TCU129, with a total value of $1.961\times10^{20}$ Nm. From local seismic data, Chi et al. (2001) obtained $M_o = 4.1\times10^{20}$ Nm. Together with local and teleseismic data, Ma et al. (2001) got

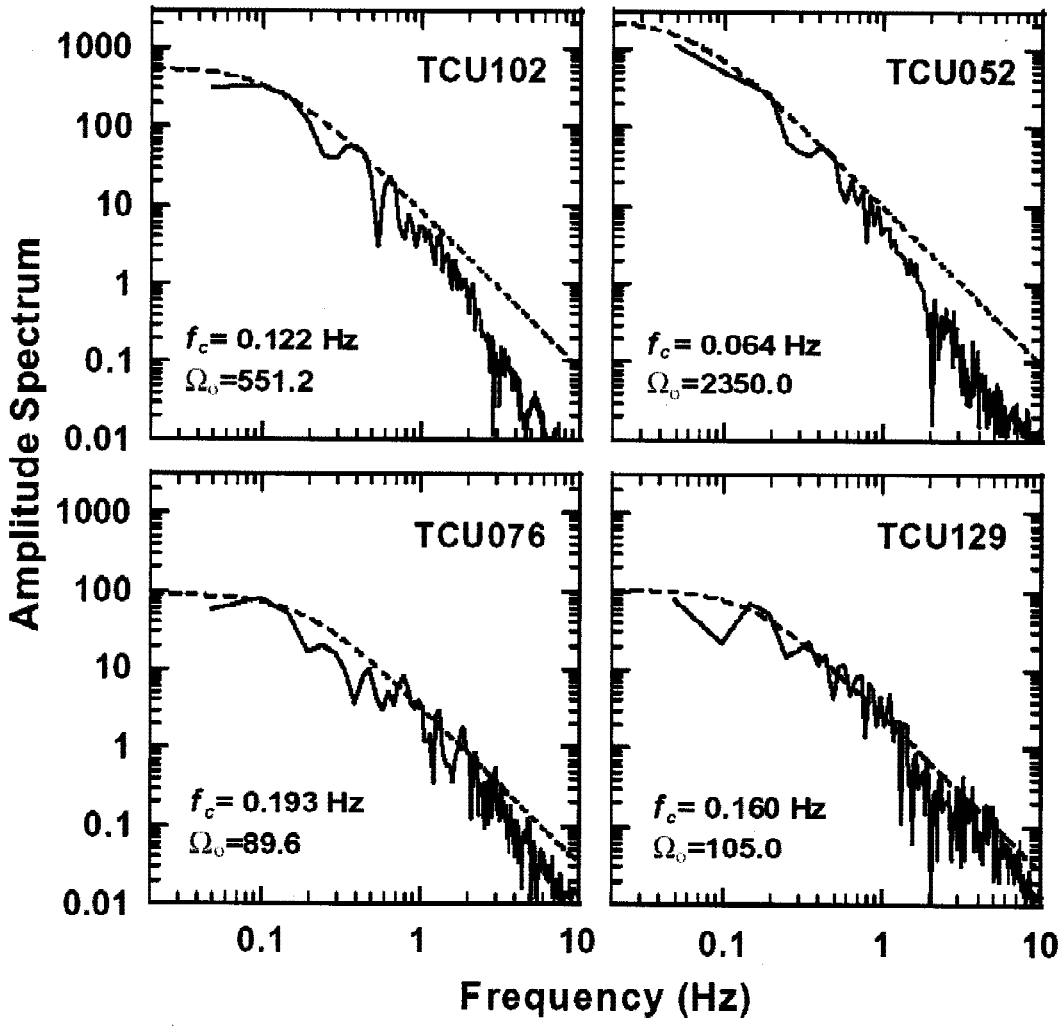


*Fig. 5.* The displacement spectra at four near-fault sites.

$M_o = 2.3\times10^{20}$ Nm. From GPS data, Hsu (2004) obtained $M_o = 2.8\times10^{20}$ Nm, and Wang et al. (2004) obtained $M_o = (3.2-3.6)\times10^{20}$ Nm based on different slip models. From the source slip model by Domingaez et al. (2003), Wang (2005b) obtained $M_{oN} = 8.14\times10^{19}$ Nm and $M_{oS} = 7.12\times10^{19}$ Nm, and, thus, $M_o = M_{oN} + M_{oS} = 1.53\times10^{20}$ Nm for the whole fault. Together with local seismic and GPS data, the estimated values of $M_o$ are: (a) $2.7\times10^{20}$ Nm by Wu et al. (2001); (b) $2.9\times10^{20}$ Nm by Zeng and Chen (2001); and (c) $2.7\times10^{20}$ Nm by Ji et al. (2004). From local and teleseismic data plus GPS data, Ma et al. (2001) obtained $M_o = 4.6\times10^{20}$ Nm, which is about 2 times larger than that inferred only from local and teleseismic data as mentioned above. This again shows that the GPS data affect the inference of source parameters.

(6) Static Stress Drop ($\Delta\sigma_s$) and Dynamic Stress Drop ($\Delta\sigma_d$)

From teleseismic data, Kikuchi et al. (2000) obtained $\Delta\sigma_s = 42$ bars; Ma et al. (2001) got $\Delta\sigma_s = 100$ bars and $\Delta\sigma_d = 200$ bars; and Xu et al. (2002) reported that the maximum and average values of $\Delta\sigma_d$ is 250 bars and 92 bars, respectively. From near-fault seismic data, Huang et al. (2001) reported $\Delta\sigma_d = 65$ bars for the southern segment and $\Delta\sigma_d = 300$ bars for the northern one; Hwang et al. (2001a) estimated the dynamic stress drops at three seismic stations: 184 bars at TCU102, 117 bars at TCU076, and 79 bars at TCU129. From their values, the average values of $\Delta\sigma_d$ are 112 bars for the southern segment and 200 bars for the northern one.

(7) Rupture Velocity ($V_R$)

From teleseismic data, Ma et al. (2000) inferred an increase in $V_R$ from 1.2 km sec$^{-1}$ in the south to 4.0 km sec$^{-1}$ in the north, with an average of 2.5 km sec$^{-1}$; Xu et al. (2002) reported an average $V_R$ of 2.5 km sec$^{-1}$. From teleseismic surface waves, Hwang et al. (2001b) gave $V_R = 2.27$ km sec$^{-1}$. From near-field seismic data, Chen et al. (2001) reported an increase in $V_R$ from 2.28 km sec$^{-1}$ in the south to 2.69 km sec$^{-1}$ in the north. From local seismic and GPS data, the values of $V_R$ are 2.5 km sec$^{-1}$ by Wu et al. (2001), 2.6 km sec$^{-1}$ by Zeng and Chen (2001), and 2.0 km sec$^{-1}$ by Ji et al. (2003). Using local and teleseismic data plus GPS data, Ma et al. (2001) reported $V_R = (0.75 - 0.80)\beta$, where $\beta$ is the average S-wave velocity of the source area, with an average of 2.5 km sec$^{-1}$. It is obvious that the rupture velocity increases from south to north.

In order to show the difference in the rupture velocities inferred by different group of researchers, the distance-time functions based on $V_R$ are displayed in Fig. 6: the thick solid lines for Chen et al. (2001), the thin solid lines for Ji et al. (2003), the dashed lines for Ma et al. (2001), a dotted line for Wu et al. (2001), and a dashed-dotted line for Zeng and Chen (2001). In addition, a very thin solid line displays an average rupture velocity of 2.32 km sec$^{-1}$. The slope of each line is the rupture velocity. Obviously, the fastest rupture velocity was inferred by Zeng and Chen (2001), and the slowest one was given by Ji et al. (2003), who also claimed that the values of $V_R$ were over-estimated by others and their value of 2 km sec$^{-1}$ is the optimum one.

(8) Strain Energy ($\Delta E$) and Seismic Radiation Energy ($E_s$)

Domingnez et al. (2003) inferred the slip distribution from GPS and InSAR data. Based on their slip distribution, Wang (2004) estimated the strain energies along the L- and W-directions, i.e., $\Delta E_L = 0.362 \times 10^{17}$ J and $\Delta E_W = 2.846 \times 10^{17}$ J. This gives $\Delta E_W / \Delta E_L = 7.86$, thus indicating that the strained energy released along the W-direction is much larger than that along the L-direction. Wang (2005b) also estimated the strain energy of the whole fault, that is $\Delta E = 3.208 \times 10^{17}$ J. From near-fault seismic data, Hwang et al. (2001a) reported that $E_s$ is $0.072 \times 10^{16}$ J at TCU129, $0.109 \times 10^{16}$ J at TCU076, $2.827 \times 10^{16}$ J at TCU052, and $1.155 \times 10^{16}$ J at TCU102. They also claimed that .the measured values of $E_s$ at TCU052 at the hanging wall is about 2.6 times larger than that of TCU102 at the footwall. After eliminating the finite frequency bandwidth effect as mentioned below, Wang (2004) revised the values of $E_s$ estimated by Hwang et al. (2001a). His results are: $E_{sN} = 3.981 \times 10^{16}$ J, $E_{sS} = 0.326 \times 10^{16}$ J, and

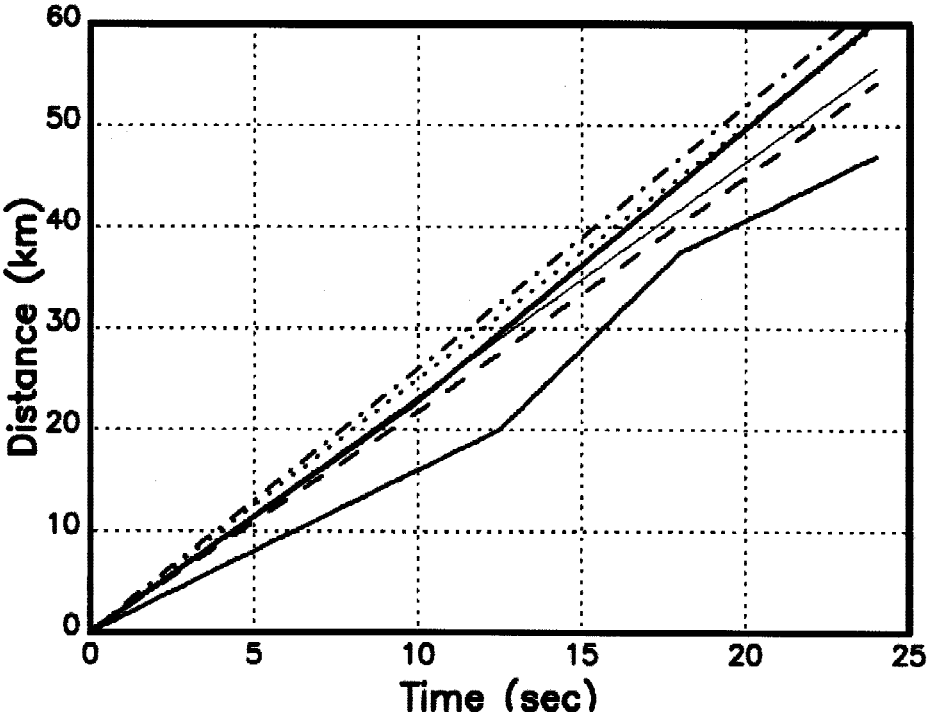


*Fig. 6.* The distance-time functions obtained by different groups of researchers based on different data: the thick solid line from Chen et al. (2001), the thin solid line from Ji et al. (2003), the dashed line from Ma et al. (2001), the dotted line from Wu et al. (2001), and the dashed-dotted line from Zeng and Chen (2001). A very thin solid line shows $V_R = 2.32$ km sec$^{-1}$.

$E_s = 4.307 \times 10^{17}$ J. From the values of $E_s$ and $\Delta E$, Wang (2004) calculated the seismic efficiency of the earthquake. The value is 0.137, which shows low seismic radiation transferred from the strained energy of the event. From far-field surface waves, Hwang et al. (2001b) got $E_s = 1.9 \times 10^{17}$ J. From far-field body waves, Venkataraman and Kanamori (2004) obtained $E_s = 8.8 \times 10^{15}$ J.

The estimated values of several source parameters for the whole fault mentioned previously are listed in Table 1. It is obvious that for a certain parameter, the values obtained by different authors based on different data are distinct. Hence, it is not easy to classify the earthquake according to the results obtained just by a single author or a group of authors based on a particular data set. In order to compare the differences in the source parameters of the northern and southern segments of the Chelungpu fault, the previously mentioned results are shown in Table 2 qualitatively. It is obvious that there are differences in the source parameters between the two segments.

Table 1. Source parameters for the whole fault plane estimated by different authors based on different methods and data sets (LS = local seismic data; TS = teleseismic data; CD = crustal deformation data)

| | D (m) | $D_{max}$ (m) | $M_o$ ($10^{20}$ Nm) | $V_R$ (km/s) | $\Delta\sigma_s$ (bars) | $\Delta\sigma_d$ (bars) | $E_s$ ($10^{16}$ J) |
|---|---|---|---|---|---|---|---|
| LS | | 8 | 4.1 | 2.3 - 2.7 | | 65 - 300 | 1.82 - 1.9 |
| TS | 3.1 | 10 | 0.5 - 5.0 | 1.2 - 4.0 | 42 - 100 | 200 - 250 | 0.88 - 1.9 |
| CD | 5.1 - 6.0 | 13.1 | 1.53 - 3.6 | | | | |
| LS+TS | | 12 | 12 | | | | |
| LS+CD | 3.8 | 20 | 2.7 - 7.3 | 2.0 - 2.6 | | | |
| LS+TS+CD | | 20 | 4.6 | (0.75 - 0.8)β | | | |

Table 2. Comparison of source parameters of the northern and southern segments.

| Source Parameters | North | South | Remarks |
|---|---|---|---|
| Peak Ground Acceleration (PGA) | Smaller | Larger | Tsai and Huang (2000) and Wang *et al.* (2002) |
| Peak Ground Velocity (PGV) | Larger | smaller | Wang et al. (2002) |
| Predominant Frequency ($f_o$) | Lower | higher | Wang et al. (2002) |
| Surface Displacement ($D_o$) | Larger | smaller | CGS (1999) and Chung and Shin (1999) |
| Average Slip (D) | Larger | smaller | Lee and Ma (1999), Chi *et al.* (2001), Kikuchi *et al.* (2000), Ma *et al.* (2001, 2002), and Zeng and Chen (2001) |
| Maximum Slip ($D_{max}$) | Larger | smaller | Wang (2004) |
| Rupture Velocity ($V_R$) | Smaller | Larger | Ma *et al.* (2001, 2002) and Chen *et al.* (2001) |
| Spectral Level ($\Omega_o$) | Higher | Lower | Hwang *et al.* (2001a) |
| Corner Frequency ($f_c$) | Lower | higher | Huang and Wang (2002) |
| Static Stress Drop ($\Delta\sigma_s$) | Larger | smaller | Huang *et al.* (2001) and Hwang *et al.* (2001a) |
| Dynamic Stress Drop ($\Delta\sigma_d$) | Larger | smaller | Hwang *et al.* (2001a) |
| Seismic Moment ($M_o$) | Larger | smaller | Hwang *et al.* (2001a) |
| Strain Energy ($\Delta E$) | Larger | smaller | Wang (2004) |
| Seismic Energy ($E_s$) | Larger | smaller | Hwang *et al.* (2001a) and Wang (2004) |
| Seismic Efficiency ($\eta$) | Larger | smaller | Wang (2004) |
| Displacement Spectra (P(f)) (0.2 Hz$\leq$f$\leq$3Hz) | $P(f)\sim f^{-3}$ | $P(f)\sim f^{-2}$ | Huang and Wang (2002) |

## 4. DISCUSSION

In addition to seismic radiation pattern, surface amplification, and seismic-wave attenuation, the site effect and finite frequency bandwidth limitation are also able to influence the estimates of source parameters. Usually, the values of source parameters estimated from local seismograms cannot match those done from teleseismic data (cf. Simth et al. 1991; Hwang et al. 2001a). This is mainly due to site and finite-frequency-bandwidth-limitation effects. Wang (2004, 2005b) did consider the two effects on the estimates of source parameters of the Chi-

Chi earthquake from local seismic data.

The value of $E_s$ could be miss-estimated from local seismograms due to the site effect as pointed out by several authors (Boatwright et al. 2002; Perez-Campos et al. 2003). The effect could be very large when the seismic station is situated at soil site. According to Boore and Joyner (1997), the amplification varies from 1.00 to 2.58 when the frequency increases from 0.01 Hz to 6.05 Hz for generic rock sites, with an average shear velocity of 620 m $sec^{-1}$ and from 1.00 to 1.15 when the frequency increases from 0.01 Hz to 8.00 Hz for generic very hard rock sites, with an average shear velocity of 2900 m $sec^{-1}$. It is obvious that the site effect could be larger at a soil site than at a very hard rock site.

Presently, there is not a frequency-dependent function to show site amplification and site attenuation in the study area. Lee et al. (2001) classified the station sites of this study to be Class C or Class D. Based on the US's criteria, the shear velocities are 360 - 760 m $sec^{-1}$ for Class C sites and 180 - 360 m $sec^{-1}$ for Class D ones. Hence, the amplification at the study sites should be larger than that given by Boore and Joyner (1997), because of the lower shear velocities based on the US's criteria. However, Lee et al. (2001) classified the sites just based on surface geology rather than the shear velocities. Except for a few station sites in the south-western part of the study, most of them are at soil or rock sites. Thus, the site effect ought to be smaller than that expected from their classification. In addition, there is a lack of frequency-dependent amplification functions to represent site effects in the Taiwan region. Hence, we did not make corrections as done by Boatwright et al. (2002) and Perez-Campos et al. (2003) from such a function. Hence, the approximated corrections are taken into account. The only indication to show site effect is the ratio of spectral acceleration to maximum ground acceleration with period obtained by Lee et al. (2001) from a huge number of data. Their results show that the site effect exists mainly in the frequency range 2 - 10 Hz, with a maximum at $f = 5$ Hz for the Class C sites, and 6 Hz for the Class D ones. From their results, we can see the amplification is between 1 and 2 when 1 Hz $< f <$ 2 Hz and less than 1 when $f <$ 1 Hz. The site condition amplifies higher-frequency signals and reduces lower-frequency ones. The average amplification is about 1.5 for $f >$ 1 Hz and about 0.8 for $f <$ 1 Hz. For the squared velocities and displacements, as shown in Eqs. (8) and (9), the site effect would lead to amplifications of, on average, up to 2.25 when $f >$ 1 Hz and 0.64 when $f <$ 1 Hz. Obviously the site effect would only have some influences on the measurements of the source parameters. Of course, if the signals with $f >$ 6 Hz could be taken into account, the estimated results would be better. Meanwhile, a fact that the spectral amplitudes of the Chi-Chi earthquake remarkably fall out when $f >$ 3 Hz also decreases the site effect. Whatever the case, it is necessary to study frequency-dependent site effect on estimates of source parameters when seismograms recorded at soil sites are applied. Recently, Huang et al. (2005) evaluated the frequency-dependent site amplifications from well-logging data done at numerous seismic stations in central Taiwan. However, since most of the wells are shallower than 50 meters, only the values at high frequencies were obtained. Hence, corrections cannot be made now.

Seismograms are affected by instrument response, noise, and the finite frequency bandwidth of a filter. In principal, $E_s$ must be measured in the overall frequency band of 0 - $\infty$ Hz. But, in practice the measurement can be made only in a finite frequency band from $f_l$ to $f_u$. Errors caused by finite frequency bandwidth limitation must be considered. However, Hwang

et al. (2001a) did not make this correction. Wang (2004) studied the effect on the evaluation of $E_s$ based on the $\omega$-squared source model. Inserting Eq. (2) into Eq. (9) leads to:

$$I_V = 2\Omega^2 \int 2\pi f^2 [1 + (f/f_c)^2]^{-2} df \quad , \tag{13}$$

where the range of the integral is from $f_l$ to $f_u$, with $f_l < f_c < f_u$. In Eq. (13) $\Omega$ is regarded as a constant and put outside the integral because it can be measured directly from the low-frequency spectral level. Thus, Eq. (13) becomes:

$$I_V = \Omega^2 (2\pi)^2 f_c^3 \{-(f_u/f_c)/[1 + (f_u/f_c)^2] + (f_l/f_c)/[1 + (f_l/f_c)^2] + \tan^{-1}(f_u/f_c) - \tan^{-1}(f_l/f_c)\} . \tag{14}$$

Define $I_{Vo} = \Omega^2 (2\pi f_c)^3 / 4$ and $\kappa = (2/\pi)\{-(f_u/f_c)/[1 + (f_u/f_c)^2] + (f_l/f_c)/[1 + (f_l/f_c)^2] + \tan^{-1}(f_u/f_c) - \tan^{-1}(f_l/f_c)\}$. This gives $I_V = \kappa I_{Vo}$, and, thus, $E_s = \kappa (S_a \rho \beta I_{Vo}) = \kappa E_{so}$, where $E_{so} = S_a \rho \beta I_{Vo}$ is the value of seismic radiation energy ($E_s$) without finite frequency bandwidth limitation. The later gives $E_{so} = E_s / \kappa$. When $f_l = 0$ and $f_u \to \infty$, $\kappa = 1$, thus leading to $I_V = I_{Vo}$ and $E_s = E_{so}$. The values of fc at four stations measured by Hwang et al. (2001a) are: 0.160 Hz at TCU129, 0.193 Hz at TCU076, 0.064 Hz at TCU052, and 0.122 Hz at TCU102. Together with $f_l = 0.03$ Hz and $f_u = 3$ Hz for TCU129 and TCU076 and $f_u = 1$ Hz for TCU052 and TCU102, the values of $\kappa$ are: 0.9295 at TCU129, 0.9168 at TCU076, 0.8843 at TCU052, and 0.8403 at TCU102. Hence, from the values of $E_s$ measured by Hwang et al. (2001a), the values of $E_{so}$ are: $0.072 \times 10^{16}$ J at TCU129, $0.109 \times 10^{16}$ J at TCU076, $2.827 \times 10^{16}$ J at TCU052, and $1.155 \times 10^{16}$ J at TCU102. Obviously, finite frequency bandwidth limitation only results in a small underestimation of $E_{so}$. Considering the $\omega$-cubic source model, Wang and Huang (2005) stressed that finite frequency bandwidth limitation only causes a different effect on the $E_s$ at TCU102 due to the given values of $f_u/f_c$ and $f_l/f_c$. Of course, the difference is small.

For the near-fault displacement spectra, Huang and Wang (2002) showed an increase in the exponent $\beta$ of the source scaling law, i.e., $P(\omega) \sim \omega^{-\beta}$, from south to north. They applied the directivity effect to interpret the difference in the observed source scaling laws. In the southern fault plane (including the epicenter), the ruptures were restricted mainly in the upper crust, within an almost rectangular zone with a 40-km length and a 10-km width. On the other hand, in the northern fault plane, the ruptures took place in a larger area, with a length of 40 km and extending downward to a depth of 40 km. The slip distribution on the fault plane seems to show that at the southern section, the ruptures propagated mainly in a single-degree-of-freedom domain along the fault-length direction, while at the northern one, the ruptures occurred in a two-degree-of-freedom space. This indicates that the fault-width effect did exist at the northern section, but not at the southern one. In addition, the rise time is longer at the northern section than at the southern one. Longer rise time would result in larger amplitudes at lower frequencies. At the southernmost part of the fault plane, the rise time is very small, thus reducing the rise-time effect. Hence, there are $\omega^{-3}$-form displacement spectra at the northern stations, $\omega^{-2}$-form displacement spectra at the southern ones near the epicenter, and $\omega^{-1.63}$-form displacement spectra at southernmost ones.

In general, the values of $\Delta\sigma_s$ of large global earthquakes are in the range 10 - 100 bars, and those of $\Delta\sigma_s$ of inter-plate and intra-plate events are different (Kanamori and Anderson 1975). There are some events with abnormally large values of $\Delta\sigma_s$ up to several hundred or thousand bars, and some small events are specified with large $\Delta\sigma_d$, up to several thousand bars (cf. House and Boatwright 1980; Fukuyama et al. 1991). The abnormally large value of $\Delta\sigma_d$ might be associated with unusually high slip velocities. Both the values of $\Delta\sigma_s$ and $\Delta\sigma_d$ of the Chi-Chi earthquake are normal.

It is obvious that values of a certain source parameter estimated by different researchers are distinct. This might be due to the use of different data and methodologies. For different data, the quality and frequency bands could be different. For different methodologies, the constraints used for inversion processes could be different. Zhou et al. (2004) stressed that near-source waveform data can adequately recover the source rupture process of the shallow part of the fault, while poorly constrain the slip distribution at the deeper parts of the fault. They also claimed that the inverted results from near-source seismic data are very sensitive to the assumed geometry of the fault plane and a combination of near-source and teleseismic seismograms can provide a more complete result.

Several groups of researchers theoretically studied the reasons to produce the differences in the source parameters between the northern and southern segments of the Chelungpu fault and between the hanging wall and footwall. Numerical simulations made by Huang et al. (2002) showed different geological structures between the hanging and foot walls produce large differences in the velocities between the two walls. Hence, it is more appropriate to compare the source properties just based on data recorded only in either the hanging wall or the footwall.

Wang (2003) applied a one-body spring-slider model to approximate each segment of the Chelungpu fault and to investigate the differences in stress drops, predominant periods, displacements, velocities, and accelerations at the two segments. Results show that the displacement is capable of reflecting behavior of a ruptured area, which consists of numerous different asperities, while the predominant (or natural) period is able to display the oscillation of the major asperity on the fault plane. However, the simple model cannot interpret the differences in velocities and accelerations between the northern and southern segments of the Chelungpu fault. In order to understand the overall behavior of the fault, we need (1) accurate directly measured data and/or inverted results in the fault zone; and (2) a more comprehensive model consisting, at least, of two coupled sliders in the presence of a more complicated friction force. Wang (1995) stressed the importance of coupling between two sub-faults on earthquake ruptures. A two-body or many-body dynamic model is necessary to simulate the rupture processes of the Chi-Chi earthquake.

From a simple dynamic model, Oglesby and Day (2001) stressed that the asymmetrical dipping fault geometry could explain several observations including the hanging wall moving more than the footwall (with strongly peak velocities right at the fault trace) and a transition from predominantly thrust faulting in the south to largely left-lateral motion in the north. Dalguer et al. (2001) simulated the ground motions along a southern profile and a northern one using a 2D discrete element method. Each profile was independently modeled. The principle simulations results are: (1) The ground velocities in the frequency range 0.5 - 2 Hz are small

near the surface breaks. (2) The fault ruptures reach the surface with a velocity of 1.2 km $sec^{-1}$ in the north and 3.0 km $sec^{-1}$ in the south. (3) The displacements and velocities for the vertical and horizontal components are larger in the north than in the south. (4) The displacements and velocities for the two components are larger at the hanging wall than at the footwall.

Brodsky and Kanamori (2001) proposed that lubrication caused by fluids sped up the northern ruptures. This produced the different rupture modes in the two segments. Based on the lubrication model, Ma et al. (2003) estimated the value of the critical lubricated length ($L_c$) that is the length at which elastic deformation is comparable to the initial gap height between two fault walls, to represent the lubrication effect. If $L << L_c$, the elastic deformation of the fault walls is insignificant; on the other hand, if $L > L_c$ the elastic deformation of the fault wall becomes significant and the gap between the fault walls widens. In the areas, where slip is larger than $L_c$, the fault is stressed and lubricated. They stressed that the stations TCU068 and TCU052 are just located rightly on the top of an area with large $L_c$ (> 10 m), and, thus, there are large displacements and velocities.

Using a 3D finite difference method to solve the elastodynamic equations, Zhang et al. (2003) analyzed the relations between stress and slip on the fault plane. Results show that for most of the fault plane the slip-weakening law holds and high stress drop occurs in the areas with large slip. The simulation results are consistent with observations.

The observations of $E_{sN} = 12E_{sS}$ and $\eta_N > \eta_S$ mean that more energy was released through seismic radiation in the northern segment than in the southern one. A larger $\eta$ reflects a bigger kinetic energy and a higher slip velocity. Thus, there was a larger slip velocity in the north than in the south. This is consistent with the field observations (cf. Wang et al. 2002). There are, at least, three possible reasons to produce $\eta_N > \eta_S$. First, based on a symmetrical circular crack model proposed by Sato and Hirasawa (1973), Ide (2002) stated $\eta = E_s/\Delta E \sim (V_R/\beta)^2$. As mentioned above, Ma et al. (2001) reported $V_{RN}/\beta = 0.80$ and $V_{RS}/\beta = 0.75$. This leads to $\eta_N/\eta_S = (0.80/0.75)^2 = 1.14$. This value is about 2.85 smaller than the measured one of about 3.25. Hence, the difference in $V_R/\beta$ between the two segments is only one of the reasons to cause the difference in seismic efficiency. Other reasons must be taken into account. This needs further study.

## 5. SUMMARY

1. The predominant frequency ($f_o$) decreases from south to north, and the average value is about 1 Hz in the south and 0.2 Hz in the north.
2. The corner frequency ($f_c$) decreases and the spectral level ($\Omega_o$) increases from south to north. The average values of $f_c$ and $\Omega_o$ are, respectively, about 0.17 Hz and 97 cm-sec in the south and 0.12 Hz and 550 cm-sec in the north in the footwall and 0.064 Hz and 2350 cm-sec in the northern hanging wall.In the frequency range 0.2 - 3 Hz, the near-fault displacement spectra fall out in a form of $A(f) \sim f^{-\beta}$, and the value of $\beta$ increases from 2 in the south and 3 in the north.
3. The surface displacements are 1.0 - 11.1 m horizontally and 2 - 7.5 m vertically, with the largest ones of 11.1 m horizontally and 7.5 m vertically in the north.

4. The value of D is 4.88 m in the south and 7.15 m in the north. The average D for the whole fault is in the range 3.1 - 6 m. $D_{max}$ increases from 6 m in the south to 10 m in the north. Some authors stated that the $D_{max}$ is in the range 13.8 - 20 m.
5. The seismic moment Mo is in the range $(0.5 - 4.1) \times 10^{20}$ Nm.
6. The value of $\Delta\sigma_s$ is in the range 42 - 100 bars and that of $\Delta\sigma_d$ in the range 65 - 300 bars.
7. The values of $V_R$ are in the range 1.2 - 2.3 km $sec^{-1}$ in the south and 2.0 - 4.2 km $sec^{-1}$ in the north. The average value of $V_R$ is in the range 2.0 - 2.6 km $sec^{-1}$.
8. The strained energy is $\Delta E = 3.208 \times 10^{17}$ J and the seismic radiation energy $E_s = (0.88 - 4.307) \times 10^{16}$ J.
9. Conclusively, there are differences in the source parameters between the southern and northern segments of the Chelungpu fault. This might be due to the differences in physical and chemical properties in the two segments.

**Acknowledgments** The author thanks two anonymous reviewers for their useful comments. The study was financially supported by Academia Sinica and the National Sciences Council under grant No. NSC92-2119-M-001-012.

## REFERENCES

Aki, K., 1966: Generation and propagation of G waves from the Niigata earthquake of June 16, 1964, 2, Estimation of earthquake moment, released energy, and stress-strain drop from the G wave spectrum. *Bull. Earthq. Res. Inst., Tokyo Univ.*, **44**, 73-88.

Aki, K., 1967: Scaling law of seismic spectrum. *J. Geophys. Res.*, **72**, 1217-1231.

Aki, K., and P. G. Richards, 1980: Quantitative Seismology, W. H. Freeman and Co., San Francisco, California, 932 pp.

Anderson, J. G., 1984: The 4 September 1981 Santa Barbara Island, California, earthquake: Interpretation of strong motion data. *Bull. Seism. Soc. Am.*, **74**, 995-1010.

Anderson, J. G., P. Bodin, J. N. Brune, J. Prince, S. K. Singh, R. Quaas, and M. Onate, 1986: Strong ground motion from the Michoacan Mexico, earthquake. *Science*, **233**, 1043-1049.

Andrews, D. J., 1986: Objective determination of source parameters and similarity of earthquakes of different size. In: Das, S., J. Boatwright, C. H. Scholz, (Eds.), Earthquake Source Mechanics, Am. Geophys. Union, Washington DC, 259-267.

Boatwright, J., 1978: Detailed spectral analysis of two small New York state earthquakes. *Bull. Seism. Soc. Am.*, **68**, 1117-1131.

Boatwright, J., 1980: A spectral theory for circular seismic sources: Simple estimates of source dimension, dynamic stress drop and radiated seismic energy. *Bull. Seism. Soc. Am.*, **70**, 1-27.

Boatwright, J., 1984: Seismic estimates of stress release. *J. Geophys. Res.*, **89**, 6961-6968.

Boatwright, J., G. L. Choy, and L. C. Seekins, 2002: Regional estimates of radiated seismic energy. *Bull. Seism. Soc. Am.*, **92**, 1241-1255.

Boore, D. M., and J. Boatwright, 1984: Average body-wave radiation coefficients. *Bull. Seism. Soc. Am.*, **74**, 1615-1621.

Boore, D. M., and W. B. Joyner, 1997: Site amplifications for generic rock sites. *Bull. Seism. Soc. Am.*, **87**, 327-341.

Brune, J. N., 1970: Tectonic stress and the spectra of seismic shear waves from earthquake. *J. Geophys. Res.*, **75**, 4997-5009.

Brodsky, E. E., and H. Kanamori, 2001: Elastohydrodynamic lubrication of faults. *J. Geophys. Res.*,**106**, 16357-16374.

CGS, 1999: Geological Survey of the 921 Earthquake (in Chinese). Open-File Rept., Cent. Geol. Surv., MOEA, ROC, 315 pp.

Chan, C. H., and K. F. Ma, 2004: Association of five moderate-large earthquakes to the fault in Taiwan. *Terr. Atmos. Ocean. Sci.*, **15**, 97-110.

Chen, K. C., B. S. Huang, W. G. Huang, J. H. Wang, T. M. Chang, R. D. Hwang, H. C. Chiu, and C. C. Tsai, 2001: An observation of rupture pulses of the September 20, 1999, Chi-Chi, Taiwan, earthquake from near-field seismograms. *Bull. Seism. Soc. Am.*, **91**, 1247-1254.

Chen, W. S., K. J. Lee, L. S. Lee, D. J. Ponti, C. Prentice, Y. G. Chen, H. C. Chang, and Y. H. Lee, 2004: Paleoseismology of the Chelungpu fault during the past 1900 years. *Quat. Int.*, **115-116**, 167-176.

Chi, W. C., and D. Dreger, 2002: Finite fault inversion of the September 25, 1999 ($M_w$ = 6.4) Taiwan: Implications for GPS displacements of Chi-Chi, Taiwan, earthquake sequence. *Geophys. Res. Lett.*, **29**, 39:1-4.

Chi, W. C., and D. Dreger, 2004: Crustal deformation: Results from finite source inversion of six $M_w > 5.8$ Chi-Chi aftershocks. *J. Geophys. Res.*, **109**, B07305, 1-16.

Chi, W. C., D. Dreger, and A. Kaverina, 2001: Finite-source modeling of the 1999 Taiwan (Chi-Chi) earthquake derived from a dense strong-motion network. *Bull. Seism. Soc. Am.*, **91**, 1144-1157.

Chung, J. K., and T. C. Shin, 1999: Implications of rupture processes from the displacement distribution of strong ground motions recorded during the 21 September Chi-Chi, Taiwan, earthquake. *Terr. Atmos. Ocean. Sci.*, **10**, 777-786.

Dalguer, L. A., K. Irikula, J. D. Riera, and H. C. Chiu, 2001: Fault dynamics rupture simulations of the hypocenter area of the thrust fault of the 1999 Ch-Chi (Taiwan) earthquake. *Geophys. Res. Lett.*, **28**, 1327-1330.

Dominguez, S., J. P. Avouac, and R. Michel, 2003: Horizontal coseismic deformation of the 1999 Chi-Chi earthquake measured from SPOT satellite images: Implications for the seismic cycle along the western foothills of central Taiwan. *J. Geophys. Res.*, **108**, ESE 8: 1-19.

Dysart, P. S., J. A., and I. S. Sacks, 1988: Source parameters and scaling relations for small earthquakes in the Matsushiro region, southwest Honshu, Japan. *Bull. Seism. Soc. Am.*, **78**, 571-589.

Fletcher, J. B., 1980: Spectra from high-dynamic range digital recordings of Oroville, California aftershocks and their source parameters. *Bull. Seism. Soc. Am.*, **70**, 735-755.

Frasier, C. W., and R. G. North, 1978: Evidence for $\omega$-cube scaling from amplitudes and periods of the Rat Island sequence (1965). *Bull. Seism. Soc. Am.*, **68**, 265-282.

Fukuyama, E., S. Kinoshita, and F. Yamamizu, 1991: Unusual high-stress drop subevent during the M5.5 earthquake, the largest event of the 1989 Ito-Oki swarm activity. *Geophys. Res. Lett.*, **18**, 641-644.

House, L., and J. Boatwright, 1980: Investigation of two high stress drop earthquakes in the Shumagin seismic gap, Alaska. *J. Geophys. Res.*, **85**, 7151-7165.

Hsu, Y. J., 2004: Modeling studies on interseismic, coseismic, and postseismic deformations associated with the 1999 Chi-Chi, Taiwan, earthquake, Ph.D. Dissertation, Nat. Central Univ., 133 pp. (in Chinese)

Huang, B. S., K. C. Chen, W. G. Huang, J. H. Wang, and T. M. Chang, 2001: Numerical modeling for near-source strong ground motions of the September 20, 1999, Chi-Chi, Taiwan, earthquake. *J. Chin. Inst. Engin. Series A*, **25**, 437-446.

Huang, M. W., and J. H. Wang, 2002: Scaling of displacement spectra of the 1999 Chi-Chi, Taiwan, earthquake from near-fault seismograms. *Geophys. Res. Lett.*, **29**, 47:1-4.

Huang, M. W., J. H. Wang, R. D. Hwang, and K. C. Chen, 2002: Estimates of stress drop and apparent stress of two larger-sized aftershocks of the 1999 Chi-Chi earthquake in the Chia-Yi area. *Terr. Atmos. Ocean. Sci.*, **13**, 299-312.

Huang, M. W., J. H. Wang, H. H. Hsieh, K. L. Wen, and K. F. Ma, 2005: Frequency-dependent sites amplifications evaluated from well-logging data in central Taiwan. *Geophys. Res. Lett.*, **32**, L21302, doi:10.1029/2005GL23527.

Huang, W. G., J. H. Wang, B. S. Huang, K. C. Chen, R. D. Hwang, T. M. Chang, H. C. Chiu, and C. C. Tsai, 2001: Estimates of source parameters for the Chi-Chi, Taiwan, earthquake, based on Brune's source model. *Bull. Seism. Soc. Am.*, **91**,1190-1198.

Hwang, R. D., J. H. Wang, B. S. Huang, K. C. Chen, W. G. Huang, T. M. Chang, H. C. Chiu, and C. C. Tsai, 2001a: Estimates of stress drop from near-field seismograms of the $M_s$7.6 Chi-Chi, Taiwan, earthquake of September 20, 1999. *Bull. Seism. Soc. Am.*, **91**, 1158-1166.

Hwang, R. D., G. K. Yu, and J. H. Wang, 2001b: Rupture directivity and source-process times of the September 20, 1999 Chi-Chi, Taiwan, earthquake estimated from Rayleigh-wave phase velocity. *Earth Planets Space*, **53**, 1171-1176.

Ide, S., 2002: Estimation of radiated energy of finite-source earthquake models. *Bull. Seism. Soc. Am.*, **92**, 2994-3005.

Ji C., D. V. Helmberger, D. J. Wald, and K. F. Ma, 2003: Slip history and dynamic implications of the 1999 Chi-Chi, Taiwan, earthquake. *J. Geophys. Res.*, **108**, 2412, doi:10.1029/2002JB001764.

Kanamori, H., and D. L. Anderson, 1975: Theoretical basis of some empirical relations in seismology. *Bull. Seism. Soc. Am.*, **65**, 1073-1095.

Kanamori, H., and T. H. Heaton, 2000: Microscopic and macroscopic physics of earthquakes. In: Rundle, L. B. D. L. Turcotte, and W. Klein, (Eds.), Geocomplexity and the Physics of Earthquakes, AGU Geophys. Mono. 120, Am. Geophys. Union, Washington, D.C., 147-164.

Kikuchi, M., Y. Yagi, and Y. Yamanaka, 2000: Source process of the Chi-Chi, Taiwan, earthquake of September 21, 1999 inferred from teleseismic body waves. *Bull. Earthq. Res. Inst., Univ. Tokyo*, **75**, 1-14.

Knopoff, L., 1958: Energy release in earthquakes. *Geophys. J.*, **1**, 44-52.

Lee C. T., C. T. Cheng, C. W. Liao, and Y. B. Tsai, 2001: Site classification of Taiwan free-field strong-motion stations. *Bull. Seism. Soc. Am.*, **91**, 1283-1297.

Lee, S. J., and K. F. Ma, 2000: Rupture process of the 1999 Chi-Chi, Taiwan, earthquake from the inversion of teleseismic data. *Terr. Atmos. Ocean. Sci.*, **11**, 591-608.

Lin, A., T. Ouchi, A. Chen, and T. Maruyama, 2001: Co-seismic displacements, folding and shortening structures along the Chelungpu surface rupture zone occurred during the 1999 Chi-Chi (Taiwan) earthquake. *Tectonophys.*, **330**, 225-244.

Liu, K. S., T. C. Shin, and Y. B. Tsai, 1999: A free-field strong motion network in Taiwan: TSMIP. *Terr. Atmos. Ocean. Sci.*, **10**, 337-396.

Ma, K. F., C. T. Lee, Y. B. Tsai, T. C. Shin, and J. Mori, 1999: The Chi-Chi, Taiwan earthquake: Large surface displacements on an inland thrust fault. Eos, Tran.. *AGU*, **80**, 605-611.

Ma, K. F., T. R. Song, S. J. Lee, and H. I. Wu, 2000: Spatial slip distribution of the September 20, 1999, Chi-Chi, Taiwan, earthquake ($M_w$7.6): Inverted from teleseismic data. *Geophys. Res. Lett.*, **27**, 3417-3420.

Ma, K. F., J. Mori, S. J. Lee, and S. B. Yu, 2001: Spatial and temporal slip distribution of the Chi-Chi, Taiwan, earthquake from strong motion, teleseismic and GPS data. *Bull. Seism Soc. Am.*, **91**, 1069-1087.

Ma, K. F., E. E. Brodsky, J. Mori, C. Chen, T. R. A. Song, and H. Kanamori, 2003: Evidence for fault lubrication during the 1999 Chi-Chi, Taiwan, earthquake ($M_w$7.6). *Geophys. Res. Lett.*, **30**, dori:10.1029/2002GL015380.

Oglesby, D. D., and S. M. Day, 2001: Fault geometry and the dynamics of the 1999 Chi-Chi (Taiwan) earthquake. *Bull. Seism. Soc. Am.*, **91**, 1099-1111.

Patane, D., F. Ferrucci, E. Giampiccolo, and L. Scaramuzzino, 1997: Source scaling of microearthquakes at Mt. Etna volcano and in the Calabrian Arc (southern Italy). *Geophys. Res. Lett.*, **24**, 1879-1882.

Perez-Campos, X., S. K. Singh, and G. C. Beroza, 2003: Reconciling teleseismic and regional estimates of seismic energy. *Bull. Seism. Soc. Am.*, **93**, 2123-2130.

Rau, R. J., F. T. Wu, and T. C. Shin, 1996: Regional network focal mechanism determination using 3D velocity model and SH/P amplitude ratio. *Bull. Seism. Soc. Am.*, **86**, 1270-1283.

Sato, T., and T. Hirasawa, 1973: Body wave spectra from propagating shear cracks. *J. Phys. Earth*, **21**, 415-431.

Smith, K. D., J. N. Brune, and K. F. Priestley, 1991: The seismic spectrum, radiated energy, and Savage and Wood inequality for complex earthquakes. *Tectonophys.*, **188**, 303-320.

Shin, T. C., 2000: Some seismological aspects of the 1999 Chi-Chi earthquake in Taiwan. *Terr. Atmos. Ocean. Sci.*, **11**, 555-566.

Tsai, Y. B., and M. W. Huang, 1999: Strong ground motion characteristics of the Chi-Chi, Taiwan, earthquake of September 21, 1999. *Earthq. Engin. Engin. Seism.*, **2**, 1-21.

Venkataraman, A., and H. Kanamori, 2002: Observational constraints on the fracture energy of subduction zone earthquakes. *J. Geophys. Res.*, **109**, B05302, 1-20.

Wang, J. H., 1995: Effect of seismic coupling on the scaling of seismicity. *Geophys. J. Int*., **121**, 475-488.

Wang, J. H., 1996: Velocity-weakening friction law as a factor in controlling the frequency-magnitude relation of earthquakes. *Bull. Seism. Soc. Am*., **86**, 701-713.

Wang, J. H., 1998: Studies of earthquake seismology in Taiwan during the 1897-1996 period. *J. Geol. Soc. China*, **41**, 291-336.

Wang, J. H., 2002: A dynamical study of two one-state-variable, rate-dependent and state-dependent friction laws. *Bull. Seism. Soc. Am*., **92**, 687-694.

Wang, J. H., 2003: A one-body model of the 1999 Chi-Chi, Taiwan, earthquake. *Terr. Atmos. Ocean. Sci*., **14**, 335-342.

Wang, J. H., 2004: The seismic efficiency of the 1999 Chi-Chi, Taiwan, earthquake. *Geophys. Res. Lett.,* **31**, L10613, doi:10.1029/204GL019417.

Wang, J. H., 2005a: Earthquakes rupturing the Chelungpu fault in Taiwan are time- predictable. *Geophys. Res. Lett*., **32**, L06316, doi:10.1029/204GL021884.

Wang, J. H., 2005b: Energy release and heat generation during the 1999 Chi-Chi, Taiwan, earthquake. *J. Geophys. Res.* (submitted).

Wang, J. H., and M. W. Huang, 2005: The effects on the estimates of seismic radiation energy due to finite frequency bandwidth limitation. *J. Seism.* (submitted).

Wang, J. H., M. W. Huang, K. C. Chen, R. D. Hwang, and W. Y. Chang, 2002: Aspects of characteristics of ground motions of the 1999 Chi-Chi (Taiwan) earthquake. *J. Chin. Engin. Soc*., **25**, 507-520.

Wang, W. H., S. H. Chang, and C. H. Chen, 2001: Fault slips inverted from surface displacements during the 1999 Chi-Chi, Taiwan earthquake. *Bull. Seism. Soc. Am*., **91**, 1167-1181.

Wang, W. M., Y. M. He, and Z. X. Yau, 2004: Complexity of the coseismic rupture of 1999 Chi-Chi earthquake (Taiwan) from inversion of GPS observations. *Tectonophys*., **382**, 151-172.

Wen, K. L., H. Y. Peng, Y. B. Tsai, and K. C. Chen, 2001: Why 1 g was recorded at TCU129 site during the 1999 Chi-Chi, Taiwan earthquake? *Bull. Seism. Soc. Am*., **91**, 1255-1266.

Wu, C., M. Takeo, and S. Ide, 2001: Source Process of the Chi-Chi earthquake: A joint inversion of strong motion data and global positioning system data with a multifault model. *Bull. Seism. Soc. Am*., **91**, 1128-1143.

Xu, L. S., Y. T. Chen, T. L. Teng, and G. Patau, 2002: Temporal-spatial rupture process of the 1999 Chi-Chi earthquake from IRIS and GEOSCOPE long-period waveform data using aftershocks as empirical Green's functions. *Bull. Seism. Soc. Am*., **92**, 3210-3228.

Yoshioka, S., 2001: Coseismic slip distribution of the 1999 Chi-Chi, Taiwa, earthquake deduced from inversion analysis of GPS data. *Bull. Seism. Soc. Am*., **91**, 1182-1189.

Zeng, Y., and C. H. Chen, 2001: Fault rupture process of the 20 September 1999 Chi-Chi, Taiwan, earthquake. *Bull. Seism. Soc. Am*., **91**, 1088-1098.

Zhang, W., T. Iwata, K. Irikura, H. Sekiguchi, and M. Bouchon, 2003: Heterogeneous distribution of the dynamic source parameters of the 1999 Chi-Chi, Taiwan, earthquake. *J. Geophys. Res*., **108**, ESE 4: 1-14.

Zhou, S., K. Irikura, and X. Chen, 2004: Analysis of the reliability and resolution of the earthquake source history inferred from waveforms, taking the Chi-Chi earthquake as an example. *Geophys. J. Int*., **157**, 1217-1232.